Aligned interpolation and application to drift kinetic semi-Lagrangian simulations with oblique magnetic field in cylindrical geometry

G Latu, Michel Mehrenberger, M Ottaviani, E Sonnendrücker

Aligned interpolation and application to drift kinetic semi-Lagrangian simulations with oblique magnetic field in cylindrical geometry

G. Latu, M. Mehrenberger, M. Ottaviani, E. Sonnendrücker

December 24, 2014

Abstract

We introduce field aligned interpolation for Semi-Lagrangian schemes, adapting a method developed by Hariri-Ottaviani [7] to the semi-Lagrangian context. This approach is validated on the constant oblique advection equation and on a $4D$ drift kinetic model with oblique magnetic field in cylindrical geometry. The strength of this method is that one can reduce the number of points in the longitudinal direction. More precisely, we observe that we gain a factor $\frac{|n|}{|n+m\iota|}$ (where ι is the inverse safety factor), with respect to the classical approach, for the typical function $\sin(m\theta + n\varphi)$.

1 Introduction

In gyrokinetic simulations, it is observed that solution structures follow the field lines of the (strong) magnetic field and numerical methods have to be adapted to benefit from this fact. Different strategies exist for dealing with field alignement in gyrokinetic codes (see [9], [5] for example). We explore here an idea developed recently in [7] and adapt it in the context of a semi-Lagrangian code.

Our example of validation will be the following $4D$ drift-kinetic equation in cylindrical geometry, with oblique magnetic field. We look for $f = f(t, r, \theta, z, v)$ satisfying

$$\partial_t f + [\phi, f] + v\nabla_\parallel f - \nabla_\parallel \phi \partial_v f = 0,$$

with

$$[\phi, f] = -\frac{\partial_\theta \phi}{rB_0}\partial_r f + \frac{\partial_r \phi}{rB_0}\partial_\theta f,\ \nabla_\parallel = \mathbf{b}\cdot\nabla,$$

so that

$$\partial_t f - \frac{\partial_\theta \phi}{rB_0}\partial_r f + \left(\frac{\partial_r \phi}{rB_0} + v\frac{b_\theta}{r}\right)\partial_\theta f + v b_z \partial_z f - \left(b_\theta \frac{\partial_\theta \phi}{r} + b_z \partial_z \phi\right)\partial_v f = 0, \tag{1}$$

for $(r, \theta, z, v) \in [r_{\min}, r_{\max}] \times [0, 2\pi] \times [0, 2\pi R] \times [-v_{\max}, v_{\max}]$. The self-consistent potential $\phi = \phi(r, \theta, z)$ solves the quasi-neutral equation without zonal flow

$$-\left(\partial_r^2 \phi + \left(\frac{1}{r} + \frac{\partial_r n_0}{n_0}\right)\partial_r \phi + \frac{1}{r^2}\partial_\theta^2 \phi\right) + \frac{1}{T_e}\phi = \frac{1}{n_0}\left(\int f - f_{eq} dv\right).$$

Here the oblique magnetic field $\mathbf{B}$ whose norm is B (which can depend on r) writes

$$\mathbf{B} = B\mathbf{b},\ \mathbf{b} = b_z \hat{\mathbf{z}} + b_\theta \hat{\boldsymbol{\theta}},\ b_\theta = \frac{c}{\sqrt{1+c^2}},\ b_z = \frac{1}{\sqrt{1+c^2}},\ c = \frac{\iota r}{R},$$

and is parametrized by $B_0 := Bb_z$ and the rotational transform iota which satisfies

$$\iota = \frac{b_\theta / r}{b_z / R} = \frac{1}{q},$$

where q is called the safety factor. When $\iota = 0$, we get the classical drift kinetic model given in [6, 3] for example. A similar model has been simulated in [9], with $\iota = 0.8$ as an example, using a Particle in Cell method.
Equation (1) can be derived from the gyrokinetic equations. Note that some terms are dropped (w.r.t. [9] for example), which permits to retain the oblique feature while sticking to a same structure of equation as in the case $\iota = 0$.
The strategy that we adopt is to solve the constant oblique advection equation

$$\partial_t f + v\mathbf{b} \cdot \nabla f = 0, \tag{2}$$

that enters in equation (1) using an interpolation that is aligned along the direction of the magnetic field $\mathbf{b}$. Such strategy permits to reduce the number of points in the z-direction. Note that another possible strategy would be to adapt the grid to magnetic field lines (see [2] for example); one strength of the present approach is that the grid points do not need to be changed, which permits an easier implementation, as for example the Poisson solver (here for the quasi-neutral equation) does not need to be changed.

The numerical scheme is developed in Section 2, and numerical results are shown in Section 3: first, results on the $2D$ oblique constant advection equation, where numerical errors can be performed and then results on the $4D$ drift kinetic model with oblique magnetic field. In Section 4, we give the conclusion and the perspectives of this work. In Appendix A, we detail the derivation of (1), from the gyrokinetic equations and give the dispersion relation in Appendix B.

2 Numerical scheme

2.1 Constant oblique advection

Writing $\varphi = \frac{z}{R}$, we have to solve for $g := g(t, \theta, \varphi) = f(t, r, \theta, R\varphi, v)$, the constant oblique advection equation (2). We have

$$\partial_t f + v\nabla_\parallel f = \partial_t f + v\frac{b_\theta}{r}\partial_\theta f + vb_z\partial_z f = 0,$$

which leads to

$$\partial_t g + v\frac{b_\theta}{r}\partial_\theta g + v\frac{b_z}{R}\partial_\varphi g = \partial_t g + \tilde{v}\left(\iota\partial_\theta g + \partial_\varphi g\right) = 0, \tag{3}$$

with $\tilde{v} = \frac{vb_z}{R}$, and g is 2π periodic in θ and φ.
Let $\Delta t \in \mathbb{R}^+$, and $t_j = \ell\Delta t,\ \ell \in \mathbb{N}$. We have the relation

$$g(t_\ell + \Delta t, \theta, \varphi) = g(t_\ell, \theta - \iota\tilde{v}\Delta t, \varphi - \tilde{v}\Delta t).$$

Let $N_\theta, N_\varphi \in \mathbb{N}^*$, and $\theta_i = \frac{2\pi i}{N_\theta}$, $\varphi_j = \frac{2\pi j}{N_\varphi}$, which can be defined for $i, j \in \mathbb{R}$. We suppose to know values $g_{\ell,i,j} \simeq g(t_\ell, \theta_i, \varphi_j)$, for $i = 0, \ldots, N_\theta - 1$, $j = 0, \ldots, N_\varphi - 1$. By periodicity, we can suppose that $i, j \in \mathbb{Z}$.
We fix two integers $r \leq 0 \leq s$. For $j = 0, \ldots, N_\varphi - 1$, there exists $j_0 \in \mathbb{Z}$ and $0 \leq \beta < 1$ such that

$$\varphi_j - \tilde{v}\Delta t = \varphi_{j_0+\beta}.$$

We then define

$$\varphi_j - \tilde{v}\Delta t_k = \varphi_{j_0+k},\ k = r, \ldots, s.$$

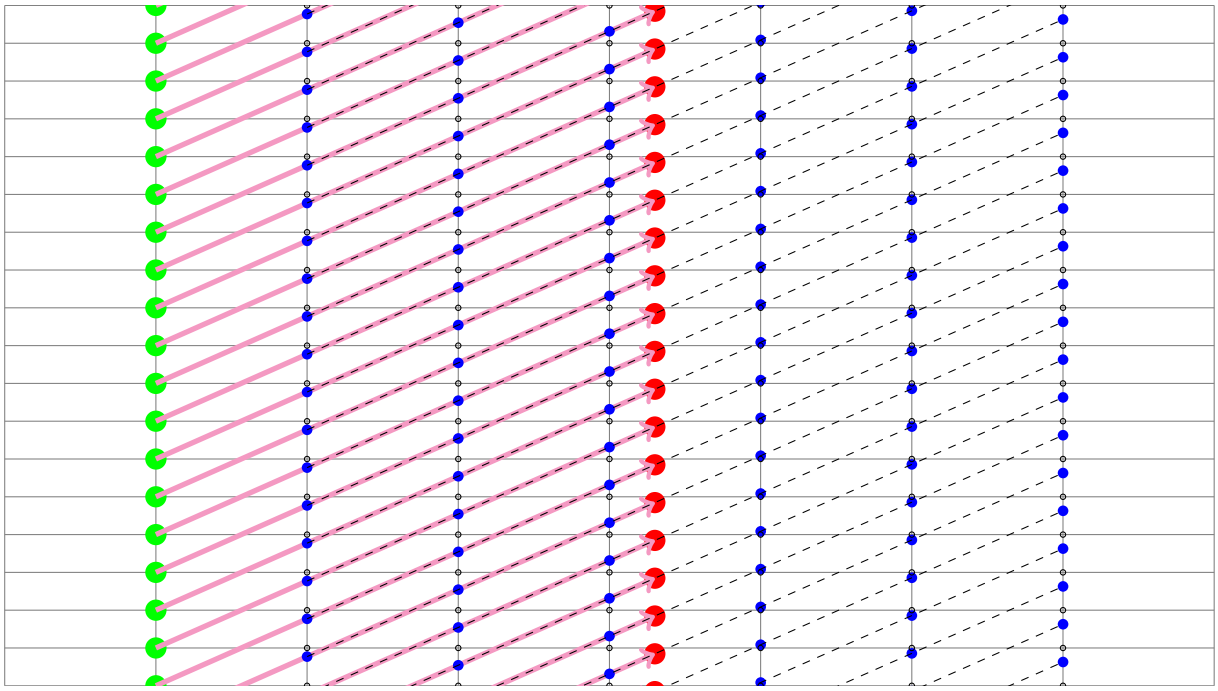

Figure 1: Schematic view of the oblique interpolation. Values at green points at time $t_{\ell+1}$ are updated through values at red points at time t_ℓ. These values are obtained by computing first values at blue points, using an interpolation in θ (vertical direction) from values at black points (constant advection), at time t_ℓ. Then values at red points are obtained from values at blue points using Lagrange interpolation along the oblique parallel direction (here LAG5).

For each $k = r, \ldots, s$, from the values

$$g_{\ell,i,j_0+k} \simeq g(t_\ell, \theta_i, \varphi_j - \tilde{v}\Delta t_k),\ i = 0, \ldots, N_\theta - 1,$$

we compute

$$\tilde{g}_{i,k} \simeq g(t_\ell, \theta_i - \iota\tilde{v}\Delta t_k, \varphi_j - \tilde{v}\Delta t_k) = g(t_\ell + \Delta t_k, \theta_i, \varphi_j),\ i = 0, \ldots, N_\theta - 1,$$

by using an interpolation in θ.
For each $i = 0, \ldots, N_\theta - 1$, from the values

$$\tilde{g}_{i,k} \simeq g(t_\ell, \theta_i - \iota\tilde{v}\Delta t_k, \varphi_j - \tilde{v}\Delta t_k), k = r, \ldots, s$$

we finally compute

$$g_{\ell+1,i,j} \simeq g(t_\ell, \theta_i - \iota\tilde{v}\Delta t, \varphi_j - \tilde{v}\Delta t),$$

using an interpolation along the parallel direction: we reconstruct a value $\tilde{g}_{i,\beta}$, from the values $\tilde{g}_{i,k}, k = r, \ldots, s$ and take $g_{\ell+1,i,j} = \tilde{g}_{i,\beta}$.
In the following, we will use Lagrange of degree $2d+1$ LAG(2d+1), for the interpolation in the parallel direction and take $r = -d,\ s = d+1$.

2.2 Drift kinetic model with oblique magnetic field

We use a classical backward semi-lagrangian (BSL) scheme as in the case where $\iota = 0$ [3]. The model is implemented in SELALIB [10] and uses a parallelization in r. Advection in z is replaced

by an advection along the parallel direction (2). The term $\mathbf{b}\cdot\nabla\phi$ is computed along the parallel direction, using a finite difference formula.

3 Numerical results

3.1 Constant oblique advection

In the case of constant oblique advection, we have to solve (3).
We consider an initial function with a well defined helicity $g = g_0(m\theta + n\varphi)$, so that

$$\mathbf{b}\cdot\nabla f = \left(m\frac{b_\theta}{r} + n\frac{b_z}{R}\right) g_0'(m\theta + n\varphi) = k_\parallel g_0'(m\theta + n\varphi),$$

where

$$k_\parallel := \frac{b_z}{R}\left(n + \iota m\right) = \frac{b_z}{qR}\left(m + qn\right),$$

In order to have $\mathbf{b}\cdot\nabla f$ bounded, we look for situations where

$$|m + qn| \leq 1,$$

as in real tokamaks, it is assumed that $k_\parallel$ will typically be in the range of $[-\frac{1}{q\,R}, \frac{1}{q\,R}]$. We will use in the sequel $g_0 = \sin$. The displacement due to advection equation has a main parameter Δt. A extended set of various Δt will be investigated because the error of one numerical scheme is much dependant on it. We choose a value for safety factor which is a non-rational surface case, $q = \sqrt{2}$. We look at four configurations for the initial functions

$$\begin{array}{lll} A : (n = 5,\ m = -7) & k_\parallel \approx 0.07 & \frac{1}{q\,R} \\ B : (n = 24,\ m = -34) & k_\parallel \approx -0.06 & \frac{1}{q\,R} \\ C : (n = 5,\ m = -6) & k_\parallel \approx 1.07 & \frac{1}{q\,R} \\ D : (n = 24,\ m = -33) & k_\parallel \approx 0.94 & \frac{1}{q\,R} \end{array} \tag{4}$$

In the Figures 2 and 3, the abcissa of the plots are N_φ, and the ordinate are the L_∞ norm which is the maximum of the difference of the function computed after one time step versus the analytical function which is here

$$f(\theta, \varphi, \Delta t) = \sin(m\left(\theta - \Delta t\right) + n\left(\varphi - q\,\Delta t\right)) \ .$$

The maximum is over the grid points and over several values of Δt. We show the results of the aligned versus the standard (non-aligned) scheme. Some parameters are fixed for this study: $N_\theta = 400$, $q = \sqrt{2}$. Note that several time steps Δt are evaluated to approximate well the maximal error one can reach for the set of parameter used (the error is varying much along with the time step).

For left-hand side plots on these two Figures, the $k_\parallel$ is near 0 and the aligned method is very accurate, even f one takes a low value for N_φ. If one considers now the right-hand side plots, the $k_\parallel$ is close to $\frac{1}{qR}$. Even if the aligned method gives lower error than standard method, the error is bigger at small N_φ compared to low $k_\parallel$.

The Fig. 2 considers lower frequency than Fig. 3. The behaviour in the two cases are similar except that there is a shift of the curves along the φ direction. This is expected, and what is interesting is that the aligned method behaves good (low error) even with low values for N_φ.

In Fig. 4, the discretisation along θ has been refined ($N_\theta = 2000$) compared to Fig. 3. The asymptotic error (at large N_φ) is lowered. The aligned method for $k_\parallel$ close to zero (left-hand side plot) is very accurate with an L_∞ error lower than 10^{-6}.

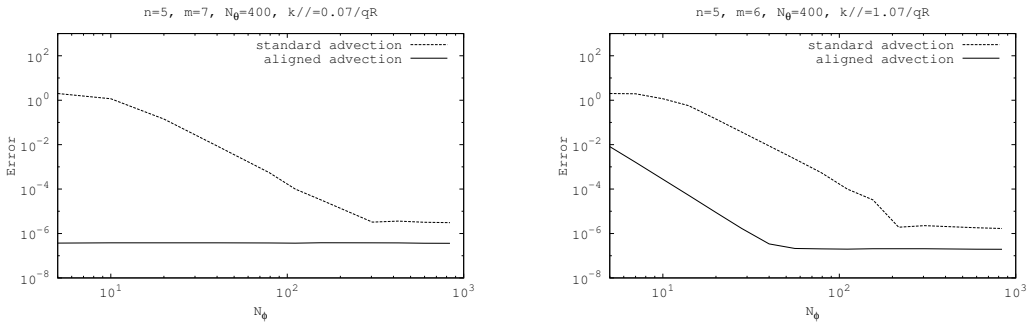

Figure 2: Error in L_∞-norm compared to the analytical solution for advection $N_\theta = 400$, $q = \sqrt{2}, n = 5$ and $m = -7$ (left), $m = -6$ (right)

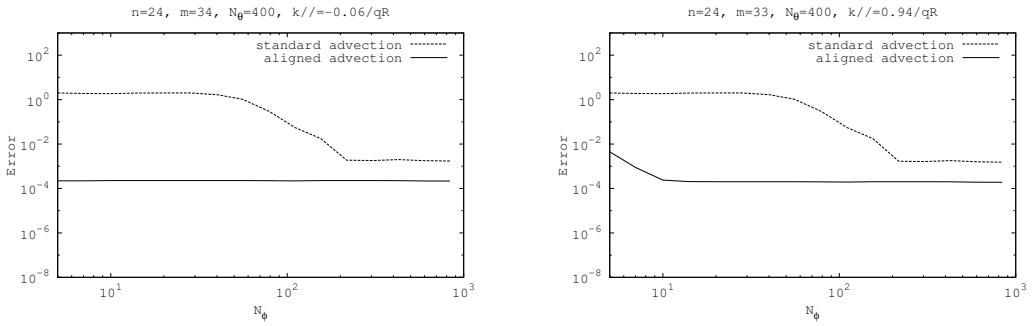

Figure 3: Error in L_∞-norm compared to the analytical solution for advection $N_\theta = 400$, $q = \sqrt{2}, n = 24$ and $m = -34$ (left), $m = -33$ (right)

A more detailed study is given on Figures 5,6,7. We first use the same configurations, but make vary the degree of interpolation in the Lagrange reconstruction: LAG3, on Figure 5 top), LAG5 on Figure 5 bottom and LAG17 on Figure 6. For the standard method, we use Lagrange interpolation in φ direction and stick to cubic splines in the θ direction, as in the case of oblique interpolation. We give the L^∞ error w.r.t. N_ϕ/n for the standard method and w.r.t. $N_\phi/|\hat{k}_\parallel|$ for the aligned method, where we have defined

$$\hat{k}_\parallel = n + m\iota.$$

Note that $k_\parallel$ and $\hat{k}_\parallel$ only differ by the constant multiplicative factor $\frac{b_z}{R}$, which enters as factor in the advection. The error does not here really depend on this factor, as we look here for maximal error over one time step of different size. In the following, we have taken $\Delta t \in \{0.1/s\}$, $s = 1, \ldots, 100$, and solved the equation

$$\partial_t g + A_1 \partial_\theta g + A_2 \partial_\varphi g,$$

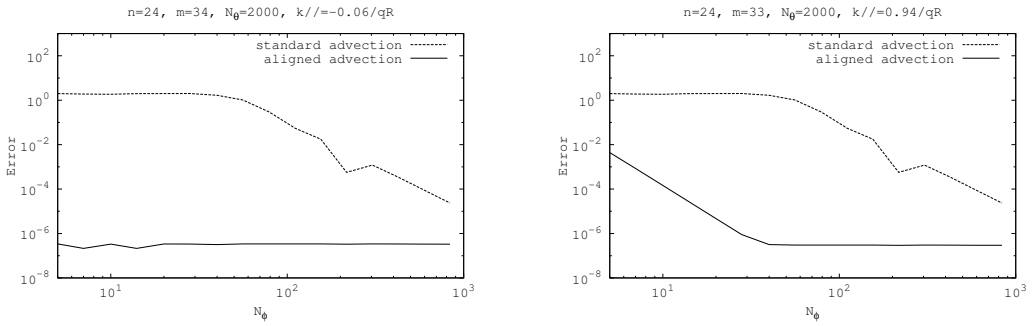

Figure 4: Error in L_∞-norm compared to the analytical solution for advection $N_\theta = 2000$, $q = \sqrt{2}, n = 24$ and $m = -34$ (left), $m = -33$ (right)

on $[0, 2\pi]^2$ with $A_1 = 1$ and $A_2 = q$. So r, R, v can be chosen so that $\tilde{v} = q$, that is

$$\frac{vb_z}{qR} = 1,\ b_z = \sqrt{1 + \left(\frac{r}{qR}\right)^2}.$$

In this way of presentation, we remark that we have three zones: a first zone, when the error does not decrease, a second zone where the error decreases according to the order of interpolation and then a third zone when the error does no more decrease which depends on $N_\theta/|m|$. Note that for a fixed degree and a given $N_\theta/|m|$, the error corresponding to the standard or aligned method lies on the *same* curve. But for a given N_ϕ, there is shift in abscissa which corresponds to the distance between $N_\varphi/|n|$ and $N_\varphi/|\hat{k}_\parallel|$. So when the error of the standard method is in the left of the curve, the error of the new method lie on the right of it. So, for example, in order to have an error around the error of discretization in θ (when the error begins to saturate: beginning of the third zone), as we are on the same curve, we typically need $\frac{N_\varphi}{|\hat{k}_\parallel|}$ points for the aligned method instead of $\frac{N_\varphi}{|n|}$ points. The factor of gain is thus

$$\frac{|n|}{|\hat{k}_\parallel|} = \frac{|n|}{|n + m\iota|}$$

On Figure 7, we fix $m = -34$ and change the values of n. Now we consider as abscissa only $N_\varphi/|m|$. We then see the same effect. We can remark that when n is smaller than $|\hat{k}_\parallel|$ (here $n = 5$ and $\hat{k}_\parallel \simeq -19$), the classical method is more accurate. For n and $\hat{k}_\parallel$ similar, both methods have the same accuracy ($n = 12$ and $\hat{k}_\parallel \simeq -12$). Then increasing n, $|\hat{k}_\parallel|$ is diminished ($n = 23$ and $\hat{k}_\parallel \simeq -1$) and the aligned method becomes more and more efficient. For $\hat{k}_\parallel \simeq 0$, we have the best result (this corresponds to the previous curve: with $n = 24$). Increasing again n, the results are still better but less and less ($n = 30$ and $\hat{k}_\parallel \simeq 6$). For $n = 100$ (not shown), we approach again the curve corresponding to $n = 12$. We have considered here LAG9, $N_\theta = 200$, except for $n = 23$, where $N_\theta = 400$. This to see, that the saturation error diminishes with N_θ (on the previous plots, we had seen that the error increases with m).

On Figures 5,6,7, we have considered the following values for N_φ:

$$N_\varphi \in A, A = \{2, 3, 4, 5, 6, 8, 9, 11, 13, 16, 19, 22, 26, 32, 38, 45, 53, 64, 76, 90, 107, 128\} \cup B,$$

$$B = \{152, 181, 215, 256, 304, 362, 430, 512, 608, 724, 861, 1024\}.$$

3.2 Drift kinetic model with oblique magnetic field

The initial function is given by

$$f(t=0,r,\theta,z,v) = f_{\rm eq}(r,v)\left[1+\epsilon\exp\left(-\frac{(r-r_p)^2}{\delta r}\right)\cos\left(m\theta+\frac{n}{R}z\right)\right],$$

where the equilibrium function is

$$f_{\rm eq}(r,v) = \frac{n_0(r)\exp(-\frac{v^2}{2T_i(r)})}{(2\pi T_i(r))^{1/2}}.$$

The radial profiles $\{T_i, T_e, n_0\}$ have the analytical expressions

$$\mathcal{P}(r) = C_{\mathcal{P}}\exp\left(-\kappa_{\mathcal{P}}\delta r_{\mathcal{P}}\tanh(\frac{r-r_p}{\delta r_{\mathcal{P}}})\right),\ \mathcal{P}\in\{T_i,T_e,n_0\},$$

where the constants are

$$C_{T_i} = C_{T_e} = 1,\ C_{n_0} = \frac{r_{\max}-r_{\min}}{\int_{r_{\min}}^{r_{\max}}\exp(-\kappa_{n_0}\delta r_{n_0}\tanh(\frac{r-r_p}{\delta r_{n_0}}))dr}.$$

Finally, we consider the parameters of [1] (MEDIUM case)

$$r_{\min}=0.1,\ r_{\max}=14.5,\ \kappa_{n_0}=0.055,\ \kappa_{T_i}=\kappa_{T_e}=0.27586,\ \delta r_{T_i}=\delta r_{T_e}=\frac{\delta r_{n_0}}{2}=1.45,$$
$$\epsilon=10^{-6},\ R=239.8081535,\ r_p=\frac{r_{\min}+r_{\max}}{2},\delta r=\frac{4\delta r_{n_0}}{\delta r_{T_i}}.$$

We take $B_0=-1$. We consider the case $\iota=0,\ n=1,\ m=15$, which leads to $k_\parallel=\frac{1}{R}$. We then consider a case $\iota=0.8,\ n=-11,\ m=15$, which leads to $k_\parallel=\frac{b_z}{R}(-11+0.8\cdot 15)=\frac{b_z}{R}$. Note that $b_z=\frac{1}{\sqrt{1+c^2}}$, with $0\le c\le \iota\frac{r_{\max}}{R}\le 0.05$, so that $|b_z-1|\le 1.25\cdot 10^{-3}$, and thus the dispersion relation which depend on m and $k_\parallel$ and not directly on n (see Appendix A) will give almost the same result, which means that both simulations should lead to similar results in the poloidal plane, at least in the linear phase (as it is also observed in [9]).
We take LAG5 for the interpolation along the parallel direction and cubic splines for the interpolation along θ. Finite differences of order 6 are used for the derivative computation along the parallel direction and cubic splines are used otherwise.
When $\iota=0$, we use the classical method with cubic splines for the interpolation along z direction. Such behavior is observed on Figure 8 and Figure 9. We see that the poloidal cut $f(t,r,\theta,z=0,v=0)$ are similar in the linear phase (Figure 8 left) and the corresponding excited modes are clearly visible in the $\theta-z$ cut $f(t,r_p,\theta,z,0)$ (Figure 9 right). After a while, we see the effect of the non linear phase. Note that we have not excited the most unstable mode (which is here $m=10,\ k_\parallel=\frac{3}{R}$).We still observe an alignment of the structures (Figure 9 bottom middle/right), and we see that the poloidal cuts are very similar considering $N_z=32$ or $N_z=64$. Note that in these figures we use raw data for the visualisation. Since the number of points in N_z is purposely low, the corresponding plots in the $\theta-z$ plane (Figure 8 middle/right and Figure 9 bottom/right) are necessarily coarse. This is not an indication of numerical problems. Indeed a better visualisation in this plane can be achieved by reconstructing the distribution function on a finer mesh using the field aligned interpolation.

4 Conclusion and perspectives

We have given some first numerical evidence that the strategy of Hariri-Ottaviani [7] works in the context of semi-Lagrangian gyrokinetic simulations. Validation has been performed on the

analytical test of the constant oblique advection and then on a drift kinetic equation with oblique magnetic field. Extension to tokamak configuration in toroidal geometry is the next step of this study. Just before submitting the first preprint, we got knowledge of the paper [8]; there, first results in this direction are already given.

Appendix A: Derivation of the model

Denoting by

$$\mathbf{B}^* = \mathbf{B} + v_\parallel \nabla \times \mathbf{b}, \quad B^*_\parallel = \mathbf{b} \cdot \mathbf{B}^* = B + v_\parallel \nabla \times \mathbf{b} \cdot \mathbf{b},$$

the gyrokinetic Vlasov equation in cartesian coordinates used in classical simulations is recalled in the review paper by Garbet et. al. [4]. In the electrostatic case it reduces to

$$\frac{\partial f}{\partial t} + \frac{d\mathbf{X}}{dt} \cdot \nabla_x f + \frac{dV_\parallel}{dt} \frac{\partial f}{\partial v_\parallel} = 0,$$

with

$$B^*_\parallel \frac{d\mathbf{X}}{dt} = V_\parallel \mathbf{B}^* + \mathbf{b} \times (\mu \nabla B + \nabla \langle \phi \rangle),$$
$$B^*_\parallel \frac{dV_\parallel}{dt} = -\mathbf{B}^* \cdot (\mu \nabla B + \nabla \langle \phi \rangle),$$

where $\langle \phi \rangle$ is the gyro-average operator applied to the electrostatic potential ϕ.
We then have, supposing that $\iota = \iota(r)$,

$$B^*_\parallel = B + \frac{2c - \iota' R c^2}{1 + c^2} v_\parallel = B + \frac{c + r c'}{1 + c^2} v_\parallel.$$

We consider for the moment $\mu = 0$, so that $\langle \phi \rangle = \phi$. We then get

$$\begin{aligned} B^*_\parallel \frac{d\mathbf{X}}{dt} &= (-(1+c^2)^{1/2} \frac{\partial_\theta \phi}{r} + c \mathbf{b} \cdot \nabla \phi) \hat{\mathbf{r}} + ((1+c^2)^{1/2} \partial_r \phi - \frac{c^2}{(1+c^2)^{1/2}} v_\parallel^2) \hat{\theta} \\ &\quad + (B^*_\parallel v_\parallel + \frac{c^3}{1+c^2} v_\parallel^2 - c \partial_r \phi) \mathbf{b} \\ B^*_\parallel \frac{dV_\parallel}{dt} &= -(B^*_\parallel + \frac{c^3}{1+c^2} v_\parallel) \mathbf{b} \cdot \nabla \phi - \frac{c^2 v_\parallel}{(1+c^2)^{1/2}} \frac{\partial_\theta \phi}{r} \end{aligned}$$

We then consider the following intermediate model

$$\begin{aligned} B^*_\parallel \frac{d\mathbf{X}}{dt} &= -(1+c^2)^{1/2} \frac{\partial_\theta \phi}{r} \hat{\mathbf{r}} + (1+c^2)^{1/2} \partial_r \phi \hat{\theta} + v_\parallel B^*_\parallel \mathbf{b} \\ \frac{dV_\parallel}{dt} &= -\mathbf{b} \cdot \nabla \phi, \end{aligned}$$

which we further simplify into

$$\begin{aligned} B \frac{d\mathbf{X}}{dt} &= -\frac{1}{(1+c^2)^{1/2}} \frac{\partial_\theta \phi}{r} \hat{\mathbf{r}} + \frac{1}{(1+c^2)^{1/2}} \partial_r \phi \hat{\theta} + v_\parallel B \mathbf{b} \\ \frac{dV_\parallel}{dt} &= -\mathbf{b} \cdot \nabla \phi. \end{aligned}$$

As we have the relation $B = B_0 (1 + c^2)^{1/2}$, we get the following model

$$\begin{aligned} \frac{d\mathbf{X}}{dt} &= -\frac{\partial_\theta \phi}{r B_0} \hat{\mathbf{r}} + \frac{\partial_r \phi}{B_0} \hat{\theta} + v_\parallel \mathbf{b} \\ \frac{dV_\parallel}{dt} &= -\mathbf{b} \cdot \nabla \phi, \end{aligned}$$

which corresponds to (1), by writing $v_\parallel$ instead of v, in order to use a shorter notation.

Appendix B: Dispersion equation

We make the following expansions:

$$f = f_0 + \varepsilon f_1 + \mathcal{O}(\varepsilon^2), \quad \phi = \phi_0 + \varepsilon\phi_1 + \mathcal{O}(\varepsilon^2)$$

with

$$f_0(r,v) = f_{eq}(r,v) = \frac{n_0(r)\exp\left(-\frac{v^2}{2T_i(r)}\right)}{(2\pi T_i(r))^{1/2}}, \quad \phi_0 = 0.$$

We obtain

$$\partial_t f_1 - \frac{\partial_\theta \phi_1}{rB_0}\partial_r f_0 + v b_z \partial_z f_1 + v\frac{b_\theta}{r}\partial_\theta f_1 - \left(b_\theta \frac{\partial_\theta \phi_1}{r} + b_z \partial_z \phi_1\right)\partial_v f_0 = \mathcal{O}(\varepsilon).$$

and

$$-\left(\partial_r^2\phi_1 + \left(\frac{1}{r} + \frac{\partial_r n_0}{n_0}\right)\partial_r\phi_1 + \frac{1}{r^2}\partial_\theta^2\phi_1\right) + \frac{1}{T_e}\phi_1 = \frac{1}{n_0}\int f_1 dv + \mathcal{O}(\varepsilon).$$

We assume that the solutions have the form :

$$f_1 = f_{m,n,\omega}(r,v)e^{i(m\theta+kz-\omega t)}, \quad \phi_1 = \phi_{m,n,\omega}(r)e^{i(m\theta+kz-\omega t)}$$

with $k = \frac{n}{R}$. Then, we obtain

$$(-\omega + kvb_z + v\frac{mb_\theta}{r})f_{m,n,\omega} = \left(\frac{m}{rB_0}\partial_r f_0 + \left(b_\theta\frac{m}{r} + b_z k\right)\partial_v f_0\right)\phi_{m,n,\omega}$$

and

$$-\left(\partial_r^2\phi_{m,n,\omega} + \left(\frac{1}{r} + \frac{\partial_r n_0}{n_0}\right)\partial_r\phi_{m,n,\omega} - \frac{m^2}{r^2}\phi_{m,n,\omega}\right) + \frac{1}{T_e}\phi_{m,n,\omega} = \frac{1}{n_0}\int f_{m,n,\omega}dv,$$

We get, as $k_\parallel = \left(b_\theta\frac{m}{r} + b_z k\right)$

$$\begin{aligned}-\left(\partial_r^2\phi_{m,n,\omega} + \left(\frac{1}{r} + \frac{\partial_r n_0}{n_0}\right)\partial_r\phi_{m,n,\omega} - \frac{m^2}{r^2}\phi_{m,n,\omega}\right) + \frac{1}{T_e}\phi_{m,n,\omega} \\ = \frac{1}{n_0}\phi_{m,n,\omega}\int \frac{\frac{m}{rB_0}\partial_r f_0 + k_\parallel \partial_v f_0}{vk_\parallel - \omega}dv\end{aligned}$$

By using the expression of f_0, we have

$$I = \int \frac{-\frac{v}{T_i} + \frac{m}{k_\parallel rB_0}\left(\frac{\partial_r n_0}{n_0} - \frac{\partial_r T_i}{2T_i} + \frac{v^2\partial_r T_i}{2T_i^2}\right)}{v - \frac{\omega}{k_\parallel}} f_0 dv.$$

We introduce for $\ell \in \mathbb{N}$:

$$I_\ell(u) = \frac{1}{n_0}\int v^\ell \frac{f_0}{v-u} f_0 dv,$$

so that

$$\frac{I}{n_0} = -\frac{1}{T_i}I_1\left(\frac{\omega}{k_\parallel}\right) + \frac{m}{k_\parallel rB_0}\left[\left(\frac{\partial_r n_0}{n_0} - \frac{\partial_r T_i}{2T_i}\right)I_0\left(\frac{\omega}{k_\parallel}\right) + \frac{\partial_r T_i}{2T_i^2}I_2\left(\frac{\omega}{k_\parallel}\right)\right].$$

We use the relations :

$$I_0 = \frac{1}{(2T_i)^{1/2}} Z\left(\frac{u}{(2T_i)^{1/2}}\right), \qquad I_1 = 1 + uI_0, \qquad I_2 = u\left(1 + uI_0\right),$$

with

$$Z(u) = \frac{1}{\sqrt{\pi}} \int \frac{\exp(-x^2)}{x-u} dx = i\sqrt{\pi}\exp(-u^2)(1 - \mathrm{erf}(-iu)),$$

$$\mathrm{erf}(x) = \frac{2}{\sqrt{\pi}} \int_0^x \exp(-t^2) dt.$$

The dispersion relation is, putting $\phi = \phi_{m,n,\omega}$, for convenience,

$$\begin{aligned} A &= -\partial_r^2 \phi - \left(\frac{1}{r} + \frac{\partial_r n_0}{n_0}\right)\partial_r \phi + \frac{m^2}{r^2}\phi + \frac{1}{T_e}\phi \\ &= \left[-\frac{1}{T_i}(1 + zZ(z)) + \frac{m}{k^* r B_0}\left(Z(z)\left(\frac{\partial_r n_0}{n_0} - \frac{\partial_r T_i}{2T_i}\right) + z(1 + zZ(z))\frac{\partial_r T_i}{T_i}\right)\right]\phi, \end{aligned}$$

with $k^* = (2T_i)^{1/2} k_\parallel$, and $z = \frac{\omega}{k^*}$, and recalling that $k_\parallel = \left(b_\theta \frac{m}{r} + b_z k\right)$. Note that the dispersion relation depends on m and $k_\parallel$ and not directly on n. This means that taking different values of ι and n but with same m and $k_\parallel$ will lead to the same dispersion relation.

References

[1] D. Coulette & N. Besse *Numerical comparisons of gyrokinetic multi-water-bag models.* JCP 248 (2013), 1–32.

[2] J. P. Braeunig, N. Crouseilles, M. Mehrenberger, E. Sonnendrücker, *Guiding-center simulations on curvilinear meshes*, Discrete and Continuous Dynamical Systems Series S, Volume 5, Number 3, June 2012.

[3] N. Crouseilles, P. Glanc, S. A. Hirstoaga, E. Madaule, M. Mehrenberger, J. Pétri, *A new fully two-dimensional conservative semi-Lagrangian method: applications on polar grids, from diocotron instability to ITG turbulence*, Eur. Phys. J. D (2014) 68: 252, topical issue of Vlasovia 2013.

[4] X. Garbet, Y. Idomura, L. Villard, T.H. Watanabe, *Gyrokinetic simulations of turbulent transport.*, Nucl. Fusion **50**, 043002 (2010).

[5] T. Görler, X. Lapillonne, S. Brunner, T. Dannert, F. Jenko, F. Merz, D. Told, *The global version of the gyrokinetic turbulence code GENE.*, J. Comput. Physics 230(18): 7053-7071 (2011).

[6] V. Grandgirard, M. Brunetti, P. Bertrand, N. Besse, X. Garbet, P. Ghendrih, G. Manfredi, Y. Sarazin, O. Sauter, E. Sonnendrücker, J. Vaclavik, L. Villard, *A drift-kinetic Semi-Lagrangian 4D code for ion turbulence simulation*, J. Comput. Phys. 217, (2006), pp. 395-423.

[7] F. Hariri, M. Ottaviani, *A flux-coordinate independent field-aligned approach to plasma turbulence simulations*, CPC 184 (2013), pp 2419–2429.

[8] J. M. Kwon, D. Yi, X. Piao, P. Kim, *Development of semi-Lagrangian gyrokinetic code for full-f turbulence simulation in general tokamak geometry,* JCP available online 15 december 2014.

[9] E. Sánchez, R. Kleiber, R. Hatzky, A. Soba, X. Sáez, F. Castejón, J. M. Cela, *Linear and nonlinear simulations using the EUTERPE gyro kinetic code*, IEEE transactions on plasma science, Vol. 38 (9), september 2010, pp. 2119–2128.

[10] SELALIB, http://selalib.gforge.inria.fr/

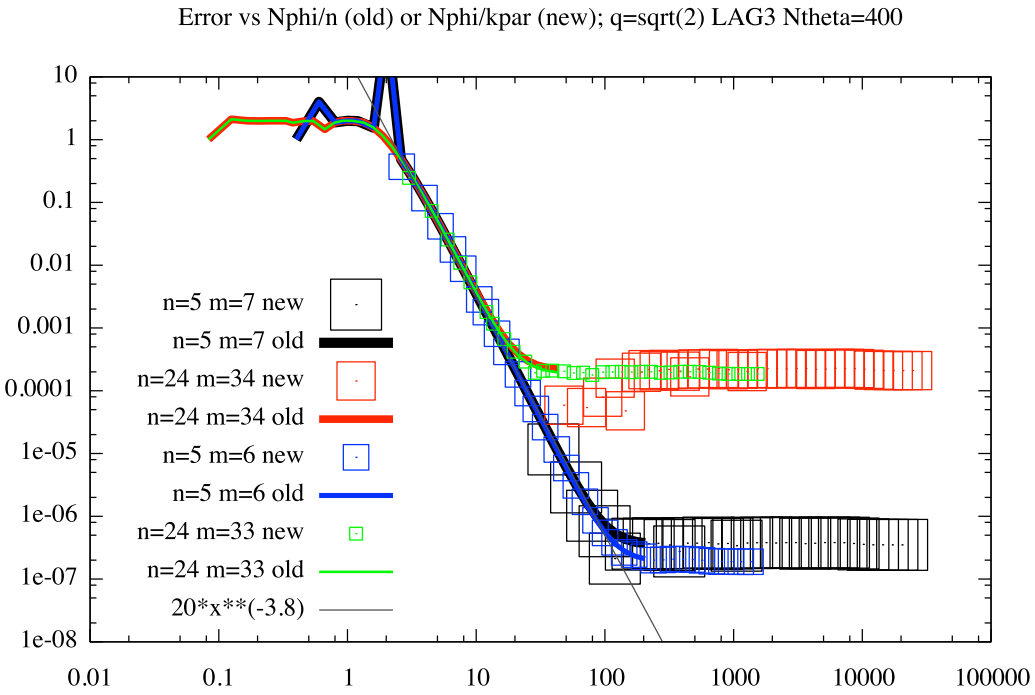

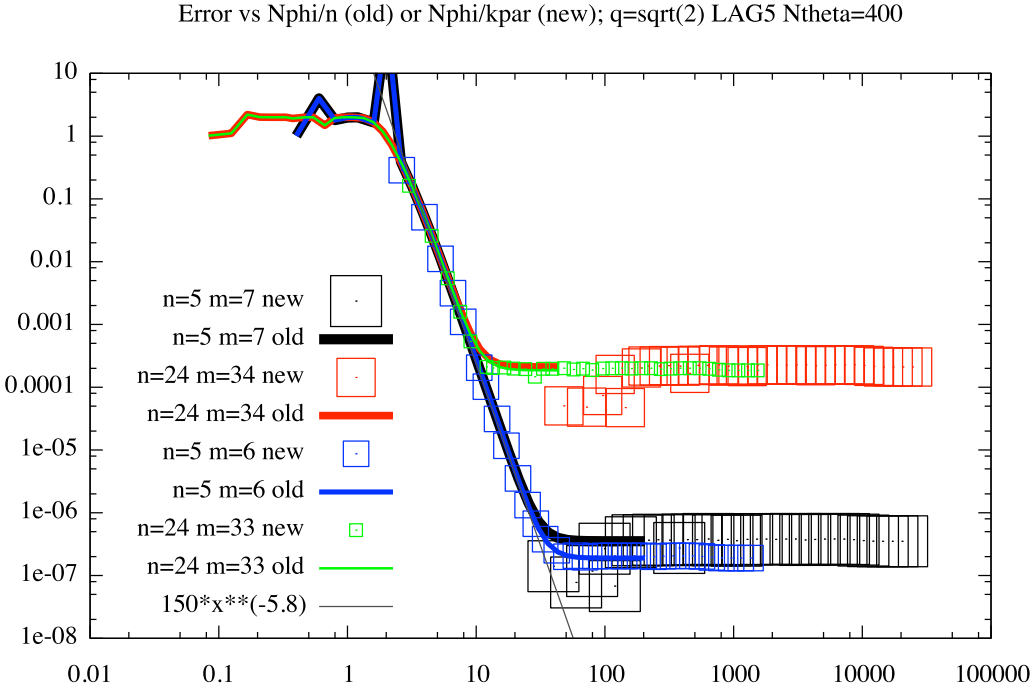

Figure 5: L^∞ error vs N_φ/n for the standard method (old) and vs $N_\varphi/|k_\||$ for the aligned method (new). Parameters are $q = \sqrt{2}$, $N_\theta = 400$. Top: LAG3; bottom: LAG5.

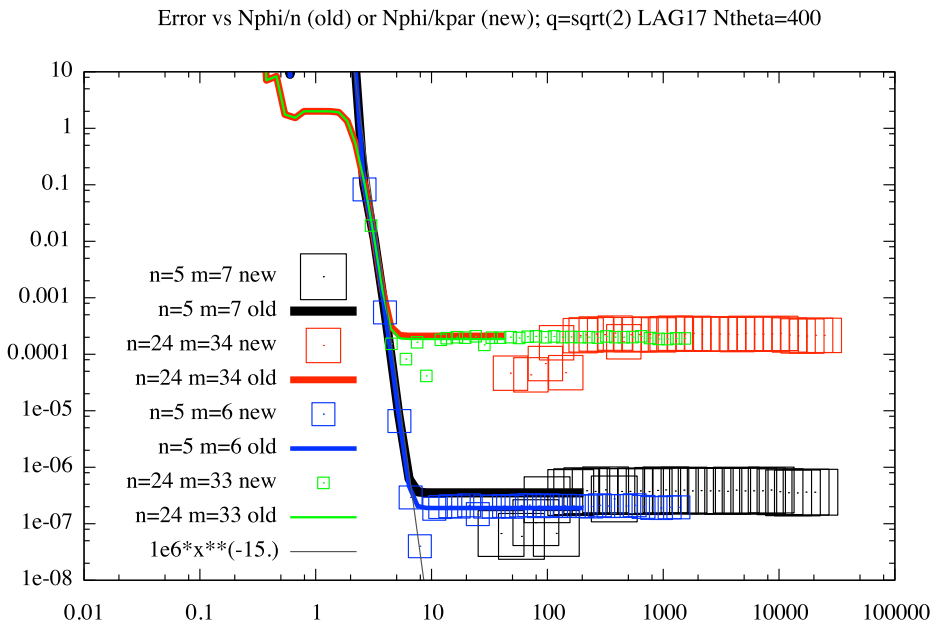

Figure 6: L^∞ error vs N_φ/n for the standard method (old) and vs $N_\varphi/|k_\parallel|$ for the aligned method (new). Parameters are $q=\sqrt{2},\ N_\theta=400$ and LAG17.

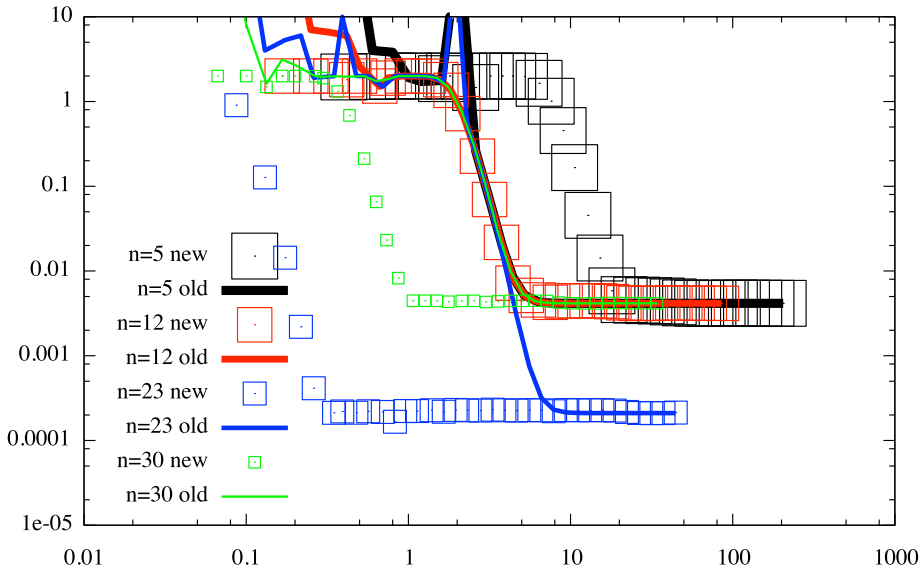

Figure 7: L^∞ error vs N_φ/n using $N_\theta=200$ (or $N_\theta=200$, when $n=23$), with parameters $q=\sqrt{2},\ m=34$, LAG9 and $n=5,12,23,30$ which corresponds to $k_\parallel\simeq -19,-12,-1,6$

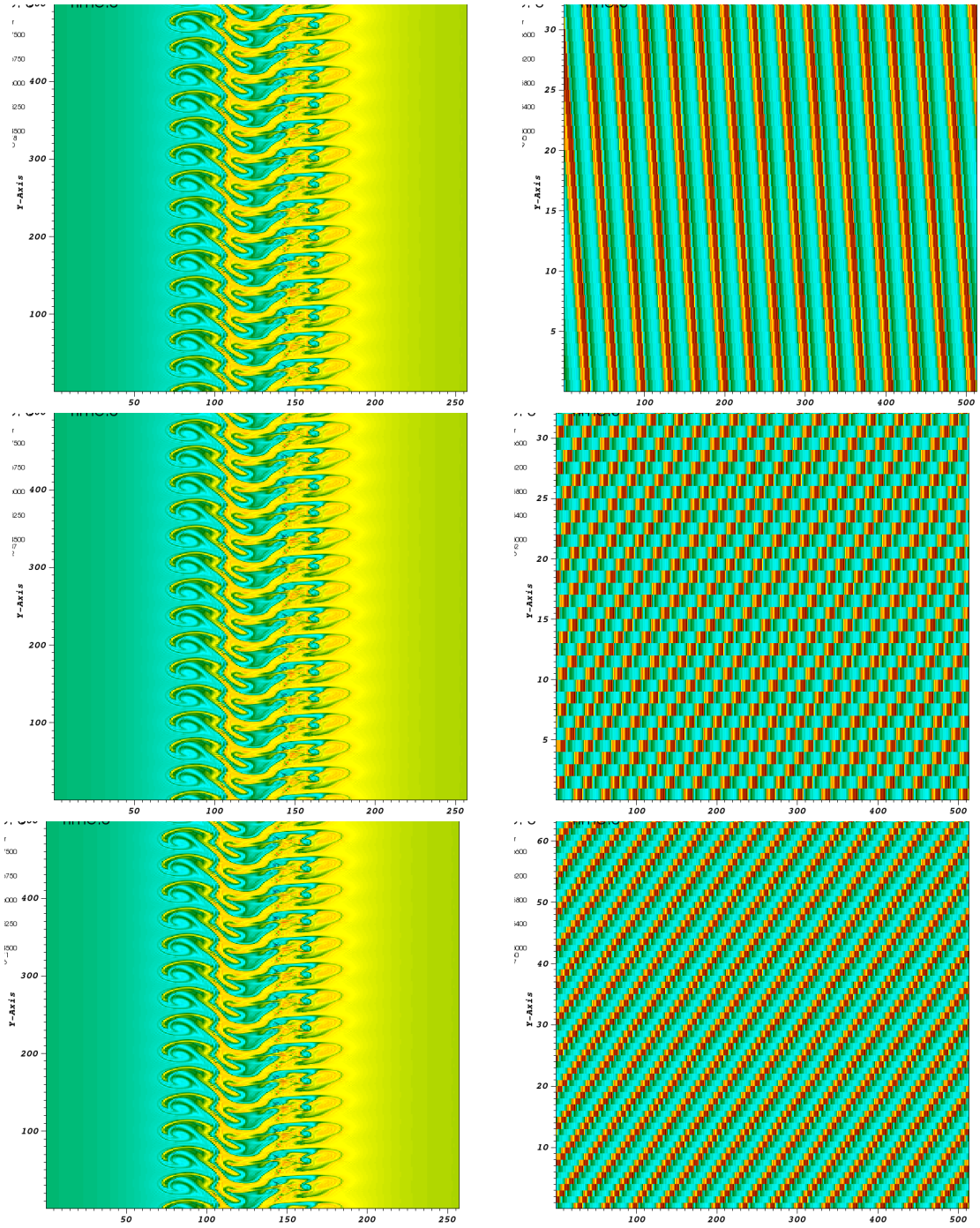

Figure 8: Poloidal cut (left) and $\theta - z$ cut (right) of distribution function at time $t = 4000$. Top: $\iota = 0,\ n = 1,\ m = 15$ on $256 \times 512 \times 32 \times 128$ grid. Middle: $\iota = 0.8,\ n = -11,\ m = 15$ on $256 \times 512 \times 32 \times 128$ grid. Bottom: $\iota = 0.8,\ n = -11,\ m = 15$ on $256 \times 512 \times 64 \times 128$ grid.

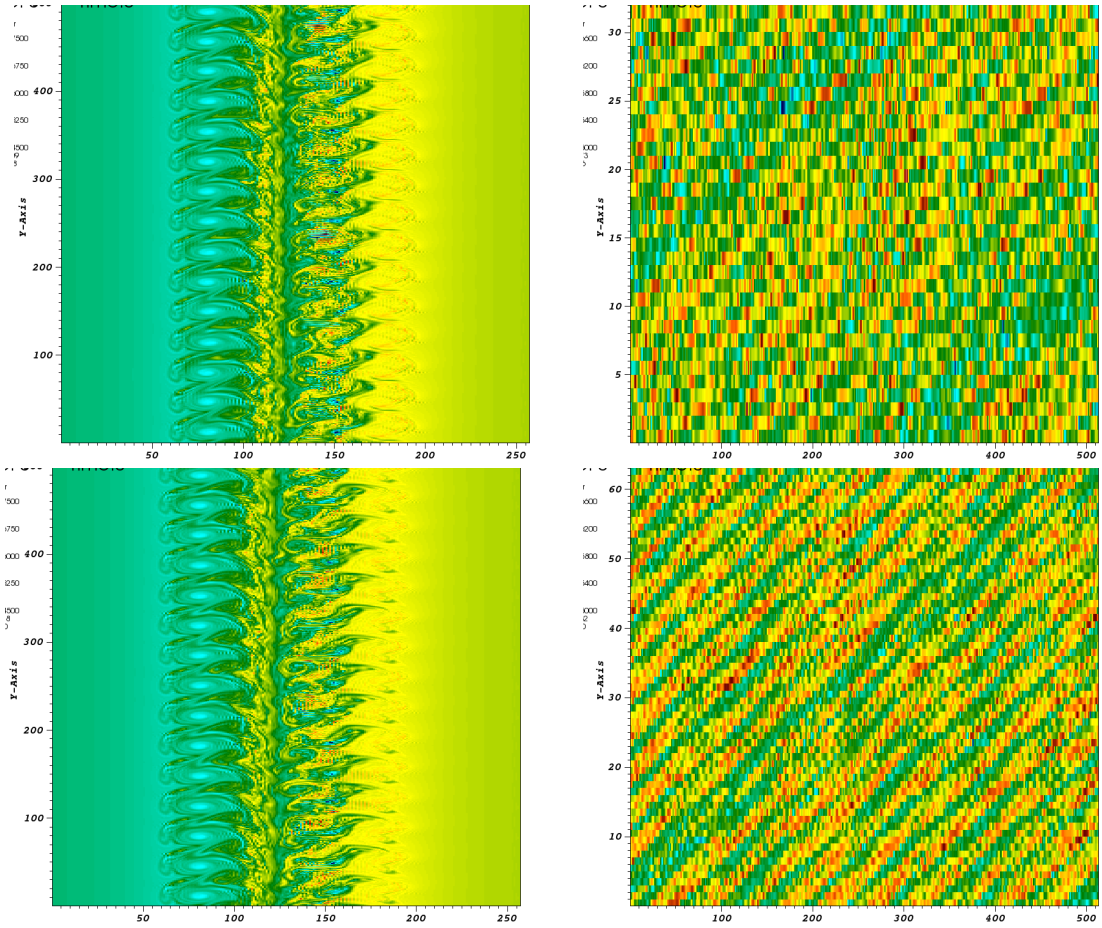

Figure 9: Poloidal cut (left) and $\theta - z$ cut (right) of distribution function at time $t = 6000$. Top: $\iota = 0.8,\ n = -11,\ m = 15$ on $256 \times 512 \times 32 \times 128$ grid. Bottom: $\iota = 0.8,\ n = -11,\ m = 15$ on $256 \times 512 \times 64 \times 128$ grid.